Journal of Alloys and Compounds 735 (2018) 131–139

Contents lists available at ScienceDirect

Journal of Alloys and Compounds

journal homepage: http://www.elsevier.com/locate/jalcom

First principles investigation of the electronic properties of graphitic carbon nitride with different building block and sheet staggered arrangement

S.P. Sun [a, *], S. Gu [a], J.H. Sun [b, **], F.F. Xia [b], G.H. Chen [c]

[a] School of Materials Engineering, Jiangsu Key Laboratory of Advanced Materials Design and Additive Manufacturing, Jiangsu University of Technology, Changzhou, 213001, China
[b] School of Chemical and Environmental Engineering, Jiangsu University of Technology, Changzhou, 213001, China
[c] Department of Chemistry, The University of Hong Kong, Hong Kong, 999077, China

ARTICLE INFO

Article history:
Received 19 July 2017
Received in revised form
31 October 2017
Accepted 5 November 2017
Available online 7 November 2017

Keywords:
g-C_3N_4
Electronic properties
Band gap
First-principles

ABSTRACT

The electronic properties of g-C_3N_4 with different building block and sheet staggered arrangement are studied by using first-principles calculations. The calculated lattice constants and band gaps of bulk g-C_3N_4 with different space group *P*-6m2, *R*3*m*, *Cmcm* and *P*6$_3$/*mmc* consistent well with the previous results. The hybrid functional HSE06 is performed to evaluate the electronic properties of graphitic carbon nitride, and it is suggested that the HSE06 hybrid functional could predict more reasonable band gap than the traditional functional. The band gaps of bulk g-C_3N_4 with *P*-6m2, *R*3*m*, *Cmcm* and *P*6$_3$/*mmc* structure are about 2.8 eV, 2.6 eV, 2.6 eV and 2.4 eV, respectively. The electronic properties of monolayer triazine- and heptazine-based structure for g-C_3N_4 are also studied, and the corresponding band gaps are 3.0 eV and 2.7 eV, respectively. Compared to the monolayer g-C_3N_4, the decreasing band gaps of bulk structures should be attributed to the band overlapping among the neighboring graphitic CN sheets. The thermodynamic properties of bulk g-C_3N_4 are also investigated, and the results show that the heptazine-based structures have larger thermal expansion coefficient and relatively smaller thermal conductivity compared to the triazine-based structures. These calculated results are suggested that not only building block but also sheet staggered arrangement has important effect on the electronic properties of g-C_3N_4. Furthermore, the charge density of monolayer g-C_3N_4 shows that C and N atoms of g-C_3N_4 sheets with different building block are all sp^2 hybridization, which is similar to that of graphite. Our results unveil that the building block and sheet staggered arrangement are effective factors to tune the electronic structure and enhance the sunlight absorption efficiency of g-C_3N_4.

1. Introduction

As the attractive functional semiconductor, two-dimensional structures, including graphene, silicene, black phosphorus, molybdenum disulfide, graphitic carbon nitride and etc, have been attracted much attention for their quantum transport, excellent photoelectric performances, and good photocatalytic properties [1–5]. Among them, g-C_3N_4 has been an important two-dimensional metal-free photocatalytic material in past two decades, which can product hydrogen by means of water dissociation [4–8]. However, the low catalytic efficiency hinders its practical application. Many efforts, especially on morphology controlling and doping with some non-metal impurities, are tried out to achieve better light absorptive properties.

A commendably comprehending of geometric structures for g-C_3N_4 is very important for morphology controlling. The graphitic C_3N_4 have different geometric structures distinguished by the two different nitrogen-linked building block in in-plane organization, including triazine-based (s-triazine units, ring of C3N3) and heptazine-based structure (tri-*s*-triazine units, tri-ring of C6N7) [9,10]. In fact, these triazine- and heptazine-based structures of bulk graphitic carbon nitrides have different space groups, including *P*-6m2, *R*3*m* and *Cmcm*. These bulk structures are

* Corresponding author.
** Corresponding author.
E-mail addresses: sunshunping@jsut.edu.cn (S.P. Sun), sunjh@jsut.edu.cn (J.H. Sun).

https://doi.org/10.1016/j.jallcom.2017.11.061
0925-8388/

composed of nitrogen-linked triazine or heptazine units, and the neighboring layers separated by weak van der Waals forces. Siller [11] has grown the large macroscopical crystalline film of triazine-based graphitic C_3N_4 (space group *P*-6m2) by ionothermal interfacial reaction, and found that triazine-based structure can be applied in the electronic device field, especially for light-emitting diode and field-effect transistor. Liu [12] proposed that doping with P atoms can effectively improve the visible-light photocatalytic properties of *P*-6m2 structure. Furthermore, it is found that the heptazine-based structure g-*t*-s-C_3N_4 (space group *Cmcm*) have a relatively high stability in graphitic CN structure [13–15]. In Zhang's earlier study [16], the other heptazine-based bulk g-C_3N_4 with space group $P6_3/mmc$ is established and investigated, and some interesting results have been obtained.

The graphitic C_3N_4 sheets can exhibit enhanced intrinsic light absorptive performances compared to the corresponding bulk structures [17], due to their lager surface area, lots of active sites, reduced photocarrier recombination, and advantaged mass transport effect. It is suggested that the morphology controlling and comprehension of geometric structure by the first-principles calculations [18,19] can help for tuning the electronic structure and enhancing the sunlight absorption efficiency. Ma [20], Lu [21] and Cui [22] have discussed the geometric, electronic and optical performance of monolayer heptazine-based graphitic C_3N_4 doped with some non-metal impurities by the first-principle calculations, and found that doping with P, S, O, and etc can enhance the visible-light absorption.

Although there are a lot of efforts on improving the photoelectric performances of g-C_3N_4 based materials in two decades, the electronic properties of the pristine g-C_3N_4 are not very clear and lacking in commendably comprehending, and the information about the effect of geometric structures on the electronic properties of graphitic carbon nitride is still far from being sufficient. In this paper, we investigated the electronic properties of g-C_3N_4 with different building block and sheet staggered arrangement using first-principles calculations, then analyzed and compared the calculated results with available experimental and theoretical results.

2. Computational methods and geometric structures

2.1. Computational methods

The triazine- and heptazine-based structure of bulk graphitic carbon nitrides with different space group *P*-6m2, *R*3*m*, *Cmcm* and $P6_3/mmc$ are investigated in this work. Fig. 1 shows four geometric structures of bulk g-C_3N_4 with different space group. These bulk g-C_3N_4 seem to have similar hexagonal unit cell, which is $a = b \neq c$, $\alpha = \beta = 90°$, $\gamma = 120°$. However, they belong to different space group and different crystal system. *P*-6m2 and $P6_3/mmc$ structures are hexagonal system, *R*3*m* structure is rhombohedral system, and *Cmcm* structure is orthorhombic system.

The present calculations were performed based on density functional theory, as implemented in VASP [23,24]. In projector augmented wave (PAW) [25] calculations, the Perdew-Burke-Ernzerhof (PBE) functional [26] was adopted, and an empirical correction method DFT-D2 [27] was employed to determined the weak van der Waals interactions. The Heyd-Scuseria-Ernzerhof hybrid functional (HSE06) [28] was implemented to examine and validate the electronic properties, the mixing parameter was 0.2. The cutoff energy was 520 eV, and the valence configurations included C-$2s^22p^2$, N-$2s^22p^3$. The Monkhorst-Pack k-points [29] $12 \times 12 \times 8$, $12 \times 12 \times 8$, $8 \times 8 \times 8$, and $8 \times 8 \times 8$ were used to integrate the Brillouin zone for *P*-6m2, *R*3*m*, *Cmcm* and $P6_3/mmc$ structures. The atomic structure symmetry was fixed, and all atomic positions in these structures were optimized until the total energy convergence was less than 1×10^{-5} eV/atom. A high-symmetry path along G (0,0,0), A (0,0,0.5), H (−0.333,0.667,0.5), K (−0.333,0.667,0), G (0,0,0), M (0,0.5,0), L (0,0.5,0.5), and H (−0.333,0.667,0.5) was used to computed the band structures for hexagonal system (*P*-6m2 and $P6_3/mmc$). A high-symmetry points along G (0,0,0), Z (0,0,0.5), T (0.5,0.5,0.5), Y (0.5,0.5,0), G (0,0,0), S (0,0.5,0), R (0,0.5,0.5), and Z (0,0,0.5) was used for orthorhombic system (*Cmcm*), and a high-symmetry points along G (0,0,0), Z (0.5,0.5,0.5), F (0.5,0.5,0), L (0,0.5,0) and G (0,0,0) was used for rhombohedral system (*R*3*m*). Every 15 k-points were generated between two neighboring points.

2.2. Geometric structures

To distinguish their structural difference, the sheet staggered arrangement of triazine- and heptazine-based structure are given in Fig. 2. It is seen that C and N atoms of g-C_3N_4 sheets of four structures with different building block are all sp^2 hybridization. The triazine-based structure consists of 3-fold coordinated C, 2-fold coordinated N (edge N), and 3-fold coordinated N (bridged N) atoms, while the heptazine-based structure includes 3-fold coordinated N (inner N) besides mentioned in triazine-based structure. And the unsaturated edge N atoms are regarded as the doping site for the substitutions site [6,12,20,22] and the active site for catalysts [15,30].

Among the triazine-based structure, there are two different configuration patterns. One configuration is stacked in an ABAB-type fashion (space group *P*-6m2). Each bridged N atoms of the

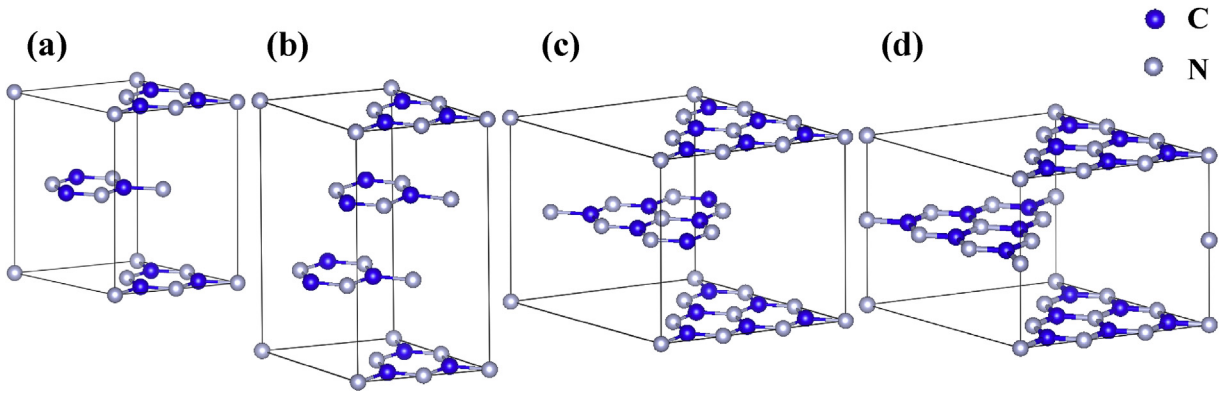

Fig. 1. The geometric models of bulk g-C_3N_4 with (a) *P*-6m2, (b) *R*3*m*, (c) *Cmcm*, and (d) $P6_3/mmc$ space groups.

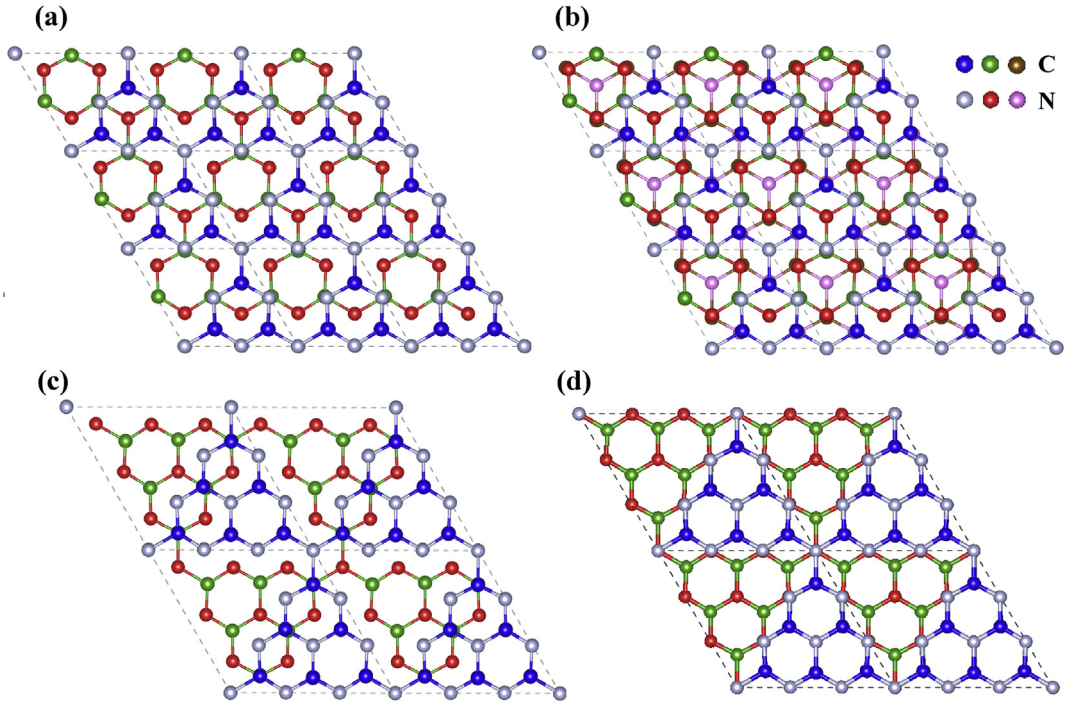

Fig. 2. The sheet staggered arrangement of bulk g-C_3N_4 with (a) *P*-6m2, (b) *R*3*m*, (c) *Cmcm* and (d) $P6_3/mmc$ space groups.

second layer are located on the top of the central ring (C3N3) of triazine units in the first layer, and the edge N atoms of the second layer are superimposed on the open hollow site in the first layer. The other configuration is an ABCABC-type staggered arrangement [11] (space group *R*3*m*), where each bridged N atoms of the latter layer is superimposed on the central ring of the former layer. The heptazine-based structure (space group *Cmcm*) has an ABAB-type staggered arrangement [9,22], and is considered as the relatively stable pristine g-C_3N_4. Its one ring (C3N3) of heptazine units in the second layer is superimposed on the central of the open hollow site in the first layer, and two edge N atoms of the second layer are superimposed on the central triazine ring in the first layer. $P6_3/mmc$ structure in Zhang's work [16] also has ABAB-type staggered arrangement and nitrogen-linked heptazine units, but it is different from *Cmcm* structure. As shown in Fig. 2d, the heptazine units of the second layer in $P6_3/mmc$ structure are almost fully located on the open hollow site in the first layer, while there is some overlapping between the neighboring layers for *Cmcm* structure. If we move the second layer of $P6_3/mmc$ structure along the body diagonal direction ($[01\bar{1}0]$) with a vector of $\frac{\sqrt{3}}{9}a$, $P6_3/mmc$ structure could be transformed to *Cmcm* structure. Owing to a weak van der Waals force among the neighboring layers, it is not difficult for monolayer stripping and interlayer slipping. Therefore, these two configurations with different sheet staggered arrangement could be occurred in graphitic CN sheets.

3. Results and discussion

3.1. Structural properties of bulk g-C_3N_4

Table 1 lists the calculated lattice constants of bulk g-C_3N_4 with different space group. The lattice constants of triazine-based structure with space group *P*-6m2 are a = 4.774 Å, c = 6.755 Å, and the average deviation of lattice constants to the available data in Refs. [31,32,35] is 1%. Moreover, the lattice constants of *R*3*m* structure are a = 4.777 Å, c = 9.256 Å. Unfortunately, there is no related structural data found in the literature for the *R*3*m* structure. From Table 1, it is obvious that *R*3*m* structure has a smaller interlayer spacing than that of *P*-6m2 structure, which could be ascribed to the interaction among the multilayers.

The lattice constants of heptazine-based structure with space group *Cmcm* are a = 7.150 Å, c = 7.059 Å, which is consistent well with others' results [13,20,22,38]. The lattice constants of $P6_3/mmc$ structure is a = 7.145 Å, c = 6.919 Å. It is noted that the calculated lattice constants of $P6_3/mmc$ structure is close to that of *Cmcm* structure, but lager than Zhang's reported results [16].

Although there are few deviations from some reported data, it is clear that the obtained lattice constants of bulk g-C_3N_4 are consistent well with the previous results listed in Table 1. The difference should be derived from the different exchange-correlation functionals and approximate approach of van der Waals interactions among the neighboring layers.

It is expected that van der Waals (vdW) interaction affects the lattice constant c of bulk C_3N_4. In fact, the distance between the C_3N_4 layers can be reduced by the vdW interaction affection [41,42], and the same phenomenon also occur in the interlayer distance of graphite [42]. We have also calculated lattice constant c of *P*-6m2 structure by the approach with no vdW correction, and found that the lattice constant c is 6.759 Å. Compared to the value without vdW correction, the lattice constant c of vdW correction 6.755 Å (listed in Table 1) has a slight decrease, which is consist with the viewpoints in Refs. [41,42]. However, the effect of vdW correction on the interlayer distance has large discrepancy among the different calculated results by different person, which should be owing to different functionals, k-points and other computational parameters.

In order to discuss the structural stability, we have computed the total energies of bulk g-C_3N_4 with different space group. Table 2 lists the total energies and relative total energies per C_3N_4 molecule of bulk g-C_3N_4 with different space group. The relative total energy per C_3N_4 molecule is corresponding to $P6_3/mmc$ structure. From Table 2, two heptazine-based structures have smaller relative total

Table 1
The calculated lattice constants and band gaps of bulk g-C_3N_4 with different space group.

space group	building block	sheet staggered arrangement	Ref.	*a*/Å	c/Å	method	vdW	*Eg*/eV
P-6m2	triazine-based	ABAB	this work	4.774	6.755	PBE + HSE	DFT-D2	2.8
			Ref. [11]	5.042	6.576	exp.	–	1.6-2.0
			Ref. [31]	4.742	6.721	LDA	–	
			Ref. [32]	4.742	6.721	PBE	–	
			Ref. [33]	4.791	6.769	PBE + HSE	–	
			Ref. [34]	4.746	6.586	LDA + GW	–	2.97
			Ref. [12]	4.774	6.134	PBE + HSE	DFT-D2	2.73
			Ref. [34]	4.72	6.64	PBE + HSE	DFT-D2	3.3
			Ref. [35]	4.74	6.69	LDA	–	1.25
			Ref. [36]	4.78	6.52	LDA	DFT-D2	1.31
*R*3*m*	triazine-based	ABCABC	this work	4.777	9.256	PBE + HSE	DFT-D2	2.6
Cmcm	heptazine-based	ABAB	this work	7.150	7.059	PBE + HSE	DFT-D2	2.6
			Ref. [37]	7.30	6.72	exp.	–	
			Ref. [4]	6.81	6.52	exp.	–	2.7
			Ref. [38]	7.133	7.086	PBE	–	
			Ref. [13]	7.13	6.92	GGA	–	
			Ref. [34]	7.083	6.871	LDA + GW	–	2.88
			Ref. [39]	6.79	6.65	PBE	DFT-D3	2.19
			Ref. [40]	7.10		PBE	–	1.0
			Ref. [20]	7.16	6.96	PW91	DFT-D2	1.19
			Ref. [22]	7.14	6.94	GGA	–	1.18
			Ref. [41]	7.13	6.01	PBE	DFT-D2	1.10
$P6_3/mmc$	heptazine-based	ABAB	this work	7.145	6.919	PBE + HSE	DFT-D2	2.4
			Ref. [16]	6.99	6.56	PBE + HSE	DFT-D2	2.71

Table 2
The total energies and relative total energies per C_3N_4 molecule of bulk g-C_3N_4 with different space group. (unit: eV).

space group	total energy	total energy per C_3N_4 molecule	relative total energy per C_3N_4 molecule
P-6m2	−156.08	−78.04	0.25
*R*3*m*	−234.29	−78.10	0.20
Cmcm	−313.04	−78.26	0.03
$P6_3/mmc$	−313.17	−78.29	0

energy than those of two triazine-based structures by about 0.2 eV per C_3N_4 molecule. It is suggested that the heptazine-based structures have better structural stability than the triazine-based structures, which agrees with the previous results [13–16].

3.2. Electronic properties of bulk g-C_3N_4

The graphitic carbon nitride system can display different structures and therefore distinct properties. To investigate these electronic properties of these geometric structures, the charge density and deformation charge density of bulk g-C_3N_4 with *P*-6m2, *R*3*m*, *Cmcm* and $P6_3/mmc$ space groups are given in Fig. 3. As mentioned in Refs. [22,43], the charge accumulation around C and N atoms is an important evidence of C–N covalent bonding. It also can be seen from Fig. 3 that C and N atoms of g-C_3N_4 sheet with different building block are all sp^2 hybridization.

Fig. 4 shows the band structures and density of states (DOS) of bulk g-C_3N_4 with *P*-6m2, *R*3*m*, *Cmcm* and $P6_3/mmc$ structures. It is seen that the band structures of two triazine-based structures exhibit some obvious difference, which should be owing to their different geometric structures and different calculated high-symmetry paths. However, the conduction band minimum (CBM) and valence band maximum (VBM) are at G point, indicating that both of the two triazine-based structures are direct semiconductors, which is consistent with Ref. [16,35,36]. The band gaps of *P*-6m2 and *R*3*m* structures are around 2.8 eV and 2.6 eV. The band gap of *R*3*m* structure is smaller slightly than that of *P*-6m2, which should be attributed to the band overlapping of complex staggered multilayers. And it is suggested that the sheet staggered arrangement can affect the electronic properties of g-C_3N_4. The band gaps of bulk g-C_3N_4 with different structures are also given in Table 1. It is seen that our results agree well with other's previous results [12,34].

For heptazine-based structures (Fig. 4c–d), the VBM locates at G point, while CBM locates at near Y point (*Cmcm*) or K point ($P6_3/mmc$), suggesting that the heptazine-based structures are indirect semiconductors [34]. According to Ref. [16], the indirect semiconductor (heptazine-based structure) is more suitable for the photocatalytic application than the direct semiconductors (triazine-based structures). Compared to the triazine-based structures, the heptazine-based structures have relatively flat band width of the VBM, which indicates their strong electron localization and low carrier mobility. The band gap of *Cmcm* structure is 2.6 eV, and smaller slightly than that of *P*-6m2 structure, which agrees with Ref. [34,36,41]. And it is clear that besides the sheet staggered arrangement, the building block also has an important influence on the electronic properties.

And the electronic properties of $P6_3/mmc$ structure calculated by our approaches are given in Fig. 4d. As shown in Fig. 4d, the electronic properties of $P6_3/mmc$ structure are also similar to those of *Cmcm* structure, due to their identical building block. And our calculated band gap of $P6_3/mmc$ structure is 2.4 eV, and smaller slightly than that of *Cmcm* structure (2.6 eV). It is suggested that the electronic properties and band gaps of g-C_3N_4 are influenced by the sheet staggered arrangement. Moreover, it is observed that our calculated band gap is smaller than 2.71 eV obtained in Ref. [16], which should be ascribed to different optimized lattice constants and mixing parameter in HSE (0.2 is used in this work, but 0.25 is used in Ref. [16]).

As show in Fig. 4 e–h, there is not different obviously from the

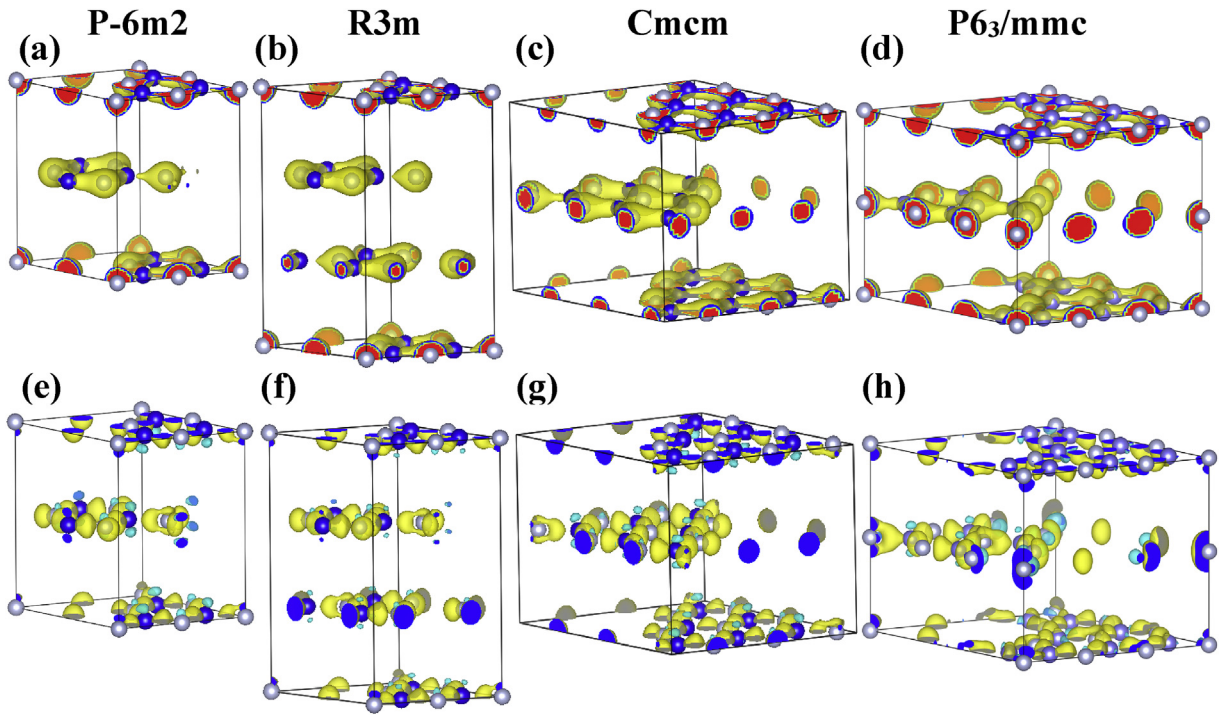

Fig. 3. (a), (b), (c) and (d) are the charge density of *P*-6m2, *R*3*m*, *Cmcm* and *P*6$_3$/*mmc* structures, respectively, and the corresponding (e), (f), (g) and (h) are the deformation charge density.

DOS for the four structures. It is clear that the VBM of four structures is dominated primarily by N-2p, and CBM is contributed by N-2p and C-2p, which agrees with that of Ref. [12]. As mentioned in Refs. [20–22,44], the C-2p states interact with the N-2p states in both valence band and conduction band, which can confirm the results of above deformation charge density (Fig. 3).

In the present work, the hybrid functional HSE06 is performed to evaluate the electronic properties of graphitic carbon nitride. If neglecting the explicit occupied orbital information, the electronic properties of semiconductor cannot be appropriately predicted. As a comparison, some available band gap results of g-C_3N_4 systems are given in Table 1. Obviously, the present band gap calculations agree well with experiments than other's results obtained by the non-hybrid functional approach in Refs. [20,22,35,36,40,41], for the latter totally ignored the effect of screened Coulomb potential. It is suggested that the HSE06 hybrid functional could predict more reasonable band gap than traditional functional.

3.3. Thermodynamic properties of bulk g-C_3N_4

The elastic properties and thermodynamic properties are important for bulk g-C_3N_4, but their related information is lacked. In this paper, the elastic properties and thermodynamic properties of *P*-6m2 and *R*3*m* structures are also calculated.

Table 3 lists the elastic constants of *P*-6m2 and *R*3*m* structures. It is seen that the elastic constants satisfy Born's criteria [45,46], which indicates that *P*-6m2 and *R*3*m* structures have good elastic stability. We can find some obvious differences from other theoretical results [42,47], which should be ascribed to the use of different functionals.

According to Voigt-Ruess-Hill approximations [46], the mechanical properties of *P*-6m2 and *R*3*m* structures can be predicted and shown in Table 4. The *Bv* and *Gv* of *P*-6m2 structure are 185.0 GPa and 149.4 GPa, and these values of *R*3*m* structure are 203.8 GPa and 167.0 GPa, respectively. The Young's modulus of *P*-6m2 and *R*3*m* structures are 180.3 GPa and 215.1 GPa, which is smaller obviously than the predicted results in Ref. [42]. However, the Poisson's ratios and G/B of *P*-6m2 and *R*3*m* structures are close to Manyali's calculated results [42]. The Poisson's ratios of *P*-6m2 and *R*3*m* structures are 0.19 and 0.21, and their G/B are 0.78 and 0.73, which indicates that *P*-6m2 and *R*3*m* structures are intrinsic brittle.

According to Ref. [48–51], the thermodynamic properties of four different structures of bulk g-C_3N_4 are investigated in this work. The heat capacity of *P*-6m2, *R*3*m*, *Cmcm* and *P*6$_3$/*mmc* structures is shown in Fig. 5. As shown in Fig. 5, the heat capacity of the bulk g-C_3N_4 structures is almost identical except C_P of *P*6$_3$/*mmc* at high temperature. The heat capacity C_V and C_P increase rapidly with T^3 at low temperature. However, C_P increases approximately linearly at high temperature, while C_V approaches a constant $3nN_Ak_B$ (~174.6 $J \cdot mol^{-1} \cdot K^{-1}$) following the Dulong–Petit limit. Ruan [41] also studied the heat capacity of a heptazine-based structure for bulk g-C_3N_4. But we can't compare our results with their calculations because their results seem to have some obvious error (their Dulong–Petit limit is 195$J \cdot mol^{-1} \cdot K^{-1}$).

Fig. 6a shows the thermal expansion coefficient of *P*-6m2, *R*3*m*, *Cmcm* and *P*6$_3$/*mmc* structures. The thermal expansion coefficient increases drastically with T^3 at low temperature, and increases approximately linearly at high temperature. It is found that the heptazine-based structures have larger thermal expansion coefficient compared to triazine-based structures. The thermal expansion coefficient of bulk g-C_3N_4 structures from small to large followed the sequence was *R*3*m*, *P*-6m2, *Cmcm* and *P*6$_3$/*mmc*, which is similar to the sequence of the above heat capacity.

Using the modified Slack's model in Refs. [52,53], the thermal conductivity of four different structures is given in Fig. 6b. Comparison with triazine-based structure, the heptazine-based structure has lower thermal conductivity because of increasing phonon scattering rate due to the larger geometric void. Mortazavi [54]

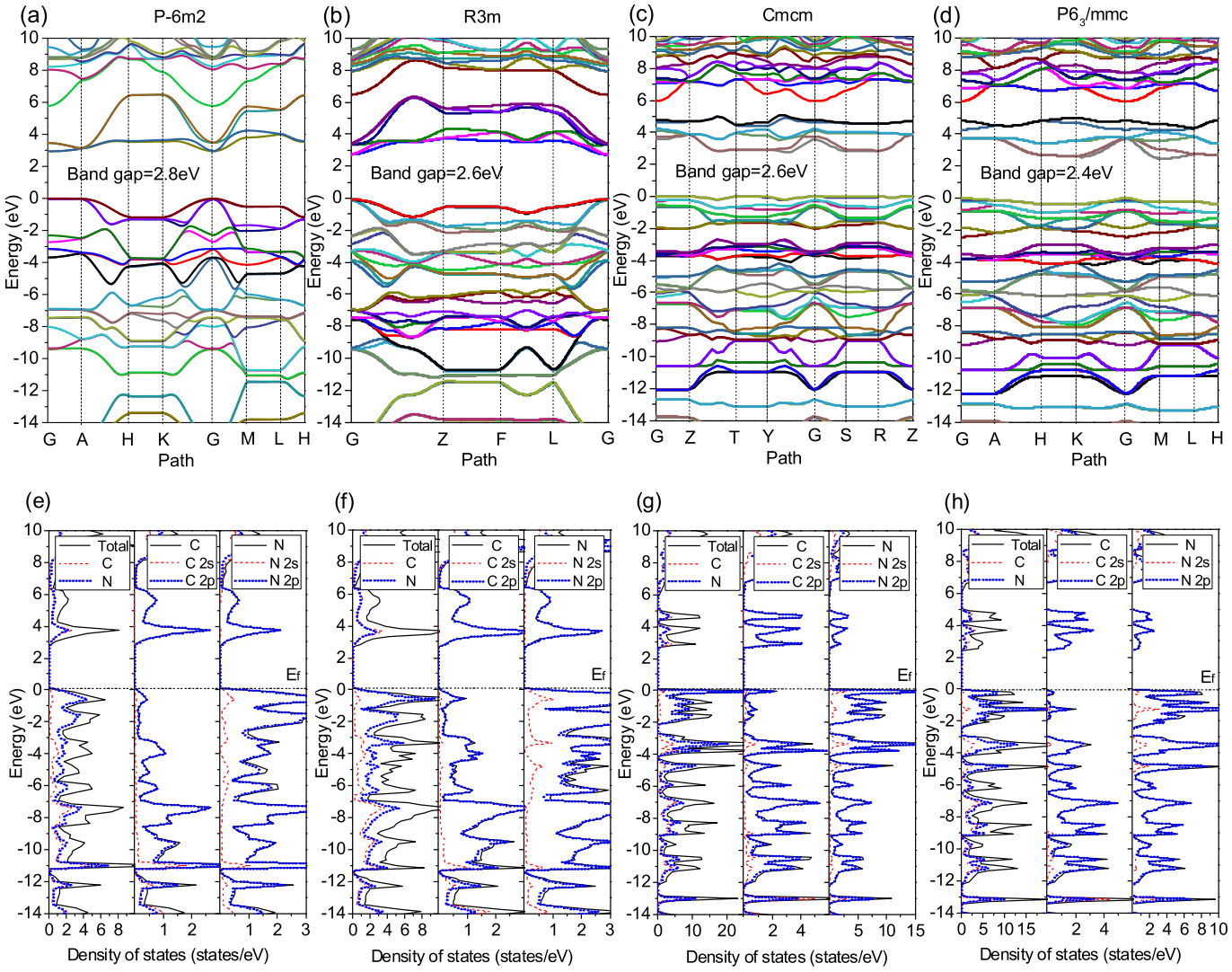

Fig. 4. (a), (b), (c) and (d) are the band structures of *P*-6m2, *R*3*m*, *Cmcm* and *P*6$_3$/*mmc* structures, respectively, and the corresponding (e), (f), (g) and (h) are the DOS.

Table 3
The elastic constants (GPa) of *P*-6m2 and *R*3*m* structures.

space group	Ref.	method	vdW	C_{11}	C_{12}	C_{13}	C_{33}	C_{44}	C_{14}
P-6m2	this work	PBE + HSE	DFT-D2	718.5	119.6	−5.2	9.7	1.0	–
	Ref. [46]	LDA	–	803	166	−3	34	5	–
		LDA	DFT-D2	904	181	−9	111	12	–
*R*3*m*	this work	PBE + HSE	DFT-D2	781.7	128.4	−8	45.4	4.9	−0.6
	Ref. [46]	LDA	–	772	235	−2	43	6	0
		LDA	DFT-D2	910	156	−8	107	10	0
	Ref. [47]	LDA	–	870	148	−3	57	14	1

Table 4
The mechanical properties of *P*-6m2 and *R*3*m* structures.

space group	Ref.	vdW	B_V	G_V	B_R	G_R	B_H	G_H	E	ν	G/B
P-6m2	this work	DFT-D2	185.0	149.4	92.2	20.8	97.1	75.7	180.3	0.19	0.78
	Ref. [46]	–	217	164					393	0.20	0.80
		DFT-D2	249	194					462	0.19	0.80
*R*3*m*	this work	DFT-D2	203.8	167.0	39.9	11.3	121.9	89.2	215.1	0.21	0.73
	Ref. [46]	–	227	146					362	0.23	0.70
		DFT-D2	245	198					469	0.18	0.70

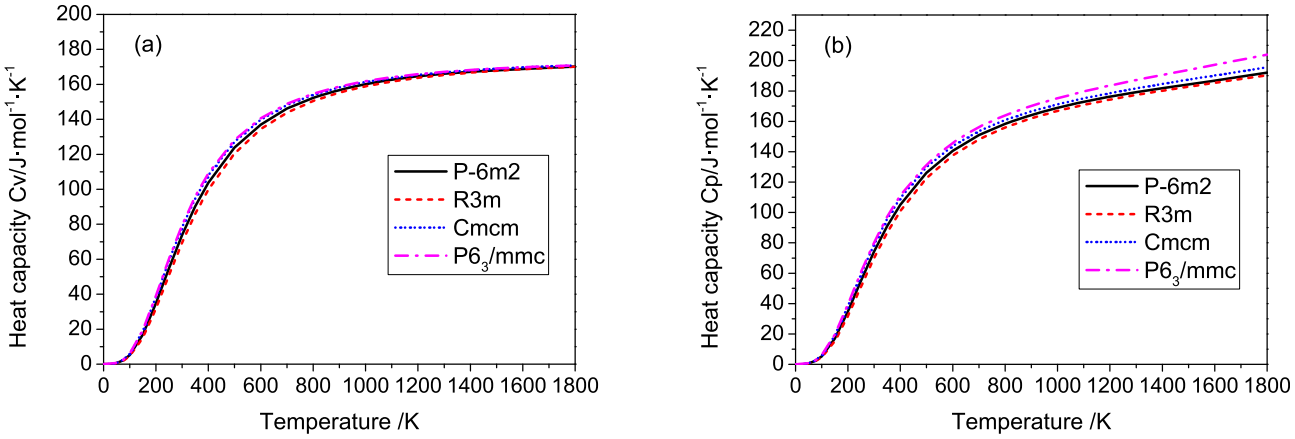

Fig. 5. The heat capacity of *P*-6m2, *R*3*m*, *Cmcm* and *P*6$_3$/*mmc* structures.

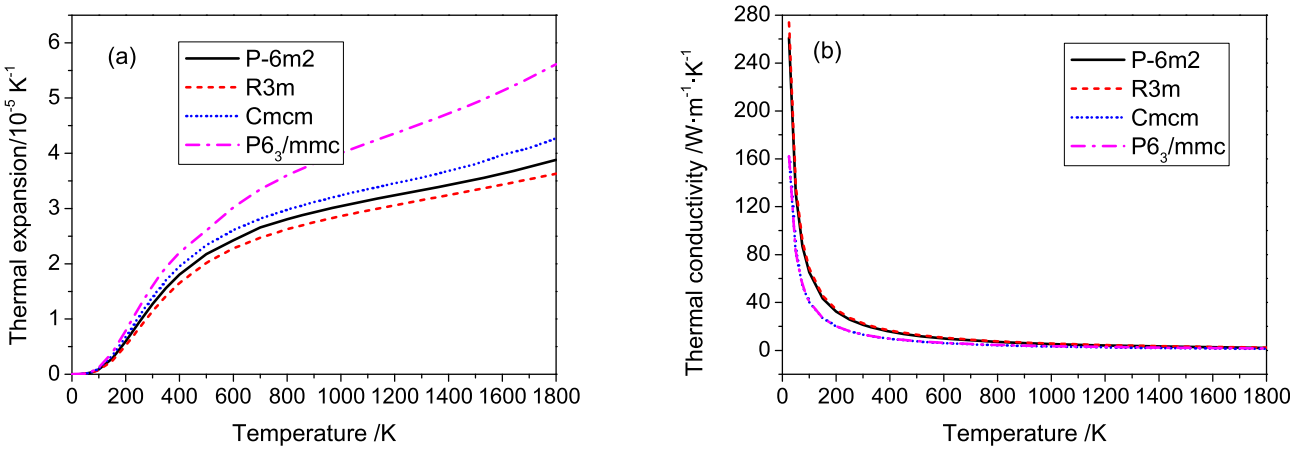

Fig. 6. The thermal expansion coefficient and thermal conductivity of *P*-6m2, *R*3*m*, *Cmcm* and *P*6$_3$/*mmc* structures.

investigated the thermal conductivity of g-C_3N_4 nanosheets by molecular dynamics approach, and discovered an identical phenomenon. As mentioned in Refs. [52,53], the modified Slack's model should underestimate the thermal conductivity at high temperature, and our calculated thermal conductivity is larger than Mortazavi's results [54].

3.4. Electronic properties of monolayer g-C_3N_4 sheets

Compared to the corresponding bulk structure, the graphitic C_3N_4 sheets exhibit remarkable feature and performance [21], and thus the graphitic CN monolayer is also investigated in this work. The g-C_3N_4 monolayer with different building block is optimized, and a vacuum space with 15 Å is used to minimize the interlayer interaction. The band structures of two monolayer g-C_3N_4 sheets are computed along the k-space high-symmetry points G (0,0,0), M (0,0.5,0), K (−0.333,0.667,0), and G (0,0,0). It is noteworthy that the g-C_3N_4 monolayer is almost flat and has no obvious buckling after the optimization for 1 × 1 pristine structure, which is in good accordance with other's results [20,38,43].

The charge density and deformation charge density of monolayer triazine- and heptazine-based structures for g-C_3N_4 are given in Fig. 7. Because the electronegativity of N (3.04) is lager than that of C (2.55), the N atoms of pristine g-C_3N_4 can attract more valence electrons compared to the C atoms. As mentioned in Ref. [20], the charge of C atoms is positive, while that of N atoms is negative. It is seen from Fig. 7 that the bonding behavior of C and N atoms of g-C_3N_4 sheet with different building block are all the same-sp^2 hybridization, which is similar to that of graphite.

The band structures and DOS of monolayer triazine- and heptazine-based structures for g-C_3N_4 are shown in Fig. 8. The band structures and DOS of monolayer structures for g-C_3N_4 are similar to those of their corresponding bulk structures, especially for the DOS. As shown in the DOS (Fig. 8c–d), the hybridization of C-2p and N-2p leads to the formation of the covalent bond, which is in good accordance with the above charge density (Fig. 7). The band gaps of monolayer triazine- and heptazine-based structure are 3.0 eV and 2.7 eV, respectively. The calculated band gaps of monolayer g-C_3N_4 sheets are larger slightly than those of bulk counterparts, which agree well with the others' findings [11,16,17,22,39]. Compared to the monolayer g-C_3N_4, the decreased band gaps of bulk structures should be ascribed to the band overlapping among the neighboring graphitic CN sheets.

The band gap of monolayer heptazine-based structure is smaller slightly than 2.80 eV [39] calculated by DFTB, but higher than the reported values 1.02 eV [15] and 1.21 eV [22] assessed by non-hybrid functional. As reported in Refs. [15,22,43], the monolayer heptazine-based structure is an indirect semiconductor, which is similar to the corresponding bulk structure. Compared to the monolayer triazine-based structure, the monolayer heptazine-based structure has a respectively small band gap, which agrees with the other's results [12,16,20].

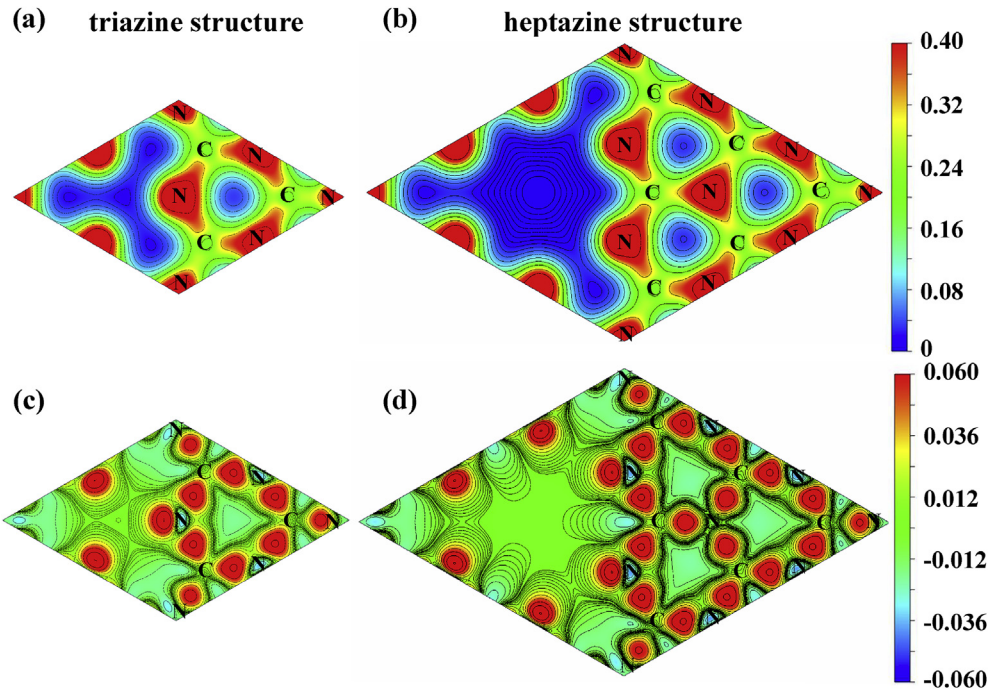

Fig. 7. (a) and (b) are the charge density of monolayer triazine- and heptazine-based structures for g-C_3N_4, respectively, and the corresponding (c) and (d) are the deformation charge density.

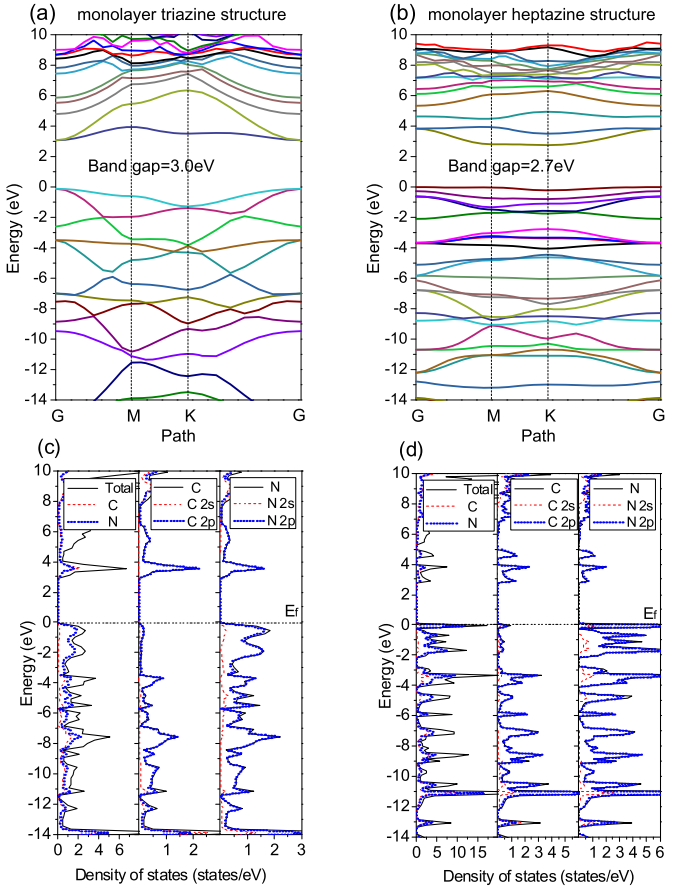

Fig. 8. (a) and (b) are the band structures of monolayer triazine- and heptazine-based structures for g-C_3N_4, respectively, and the corresponding (c) and (d) are the DOS.

It is known that these monolayer g-C_3N_4 sheets should show the different optical absorption behavior compared to bulk counterparts [16,17]. The absorption curves of four bulk structures and two monolayer g-C_3N_4 sheets is shown in Fig. 9. It is seen that these monolayer g-C_3N_4 sheets have almost the same absorption peaks to the corresponding bulk structures. However, the bulk structures have larger absorption than the monolayer g-C_3N_4 sheets. Compared with bulk g-C_3N_4, there is obvious shift towards the short wavelength side of the intrinsic absorption edge in these monolayer g-C_3N_4 sheets, which agrees well with the experiments [17]. Moreover, the absorption peaks of the heptazine-based monolayer sheet and bulk structures shift red due to smaller band gaps compared to triazine-based counterparts, which should indicate their relatively high catalytic efficiency.

Owing to the weak van der Waals force among the neighboring layers, we can achieve easily the graphitic CN sheets from bulk

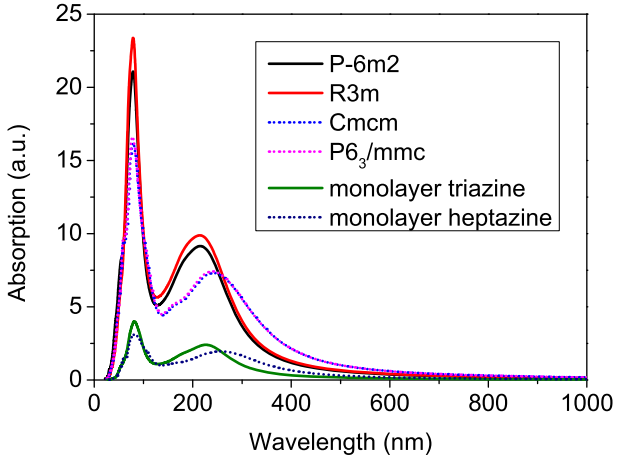

Fig. 9. The absorption curves of four bulk structures and two monolayer g-C_3N_4 sheets.

structure, which is similar to the preparation of graphene [16,17]. Compared with traditional bulk structure, two-dimensional material has large surface and appropriate band gap, which is more suitable for the photocatalytic application [16].

In summary, both the building block and sheet staggered arrangement predominantly affect the geometric structure of graphitic carbon nitride, leading to the eventual reorientation in the atomic orbitals which can in turns tune the band gap.

4. Conclusions

The electronic properties of g-C_3N_4 with different building block and sheet staggered arrangement are studied by using first-principles calculations. The calculated lattice constants of bulk g-C_3N_4 with different space group *P*-6m2, *R*3*m*, *Cmcm* and *P*6$_3$/*mmc* are consistent well with the previous results. The hybrid functional HSE06 is performed to evaluate the electronic properties of graphitic carbon nitride, and it is suggested that the HSE06 hybrid functional could predict more reasonable band gap than the traditional functional. The band gaps of bulk g-C_3N_4 with *P*-6m2, *R*3*m*, *Cmcm* and *P*6$_3$/*mmc* structure are about 2.8 eV, 2.6 eV, 2.6 eV and 2.4 eV, respectively. The electronic properties of monolayer triazine- and heptazine-based structure for g-C_3N_4 are also studied, and the corresponding band gaps are 3.0 eV and 2.7 eV, respectively. Compared to the monolayer g-C_3N_4, the decreased band gaps of bulk structures should be ascribed to the band overlapping among the neighboring graphitic CN sheets. The thermodynamic properties of bulk g-C_3N_4 are also investigated, and the results show that the heptazine-based structures have larger thermal expansion coefficient and relatively smaller thermal conductivity compared to the triazine-based structures. These calculated results are suggested that both the building block and sheet staggered arrangement have important effect on the electronic properties of g-C_3N_4. Furthermore, the charge density of monolayer g-C_3N_4 shows that C and N atoms of g-C_3N_4 sheets with different building block are all sp^2 hybridization, which is similar to that of graphite. Our results will pave the way for tuning the electronic structure and enhancing the sunlight absorption efficiency of g-C_3N_4.

Acknowledgements

This work is supported by the Natural Science Foundation of China (No. 21373103 and 51401093) and Natural Science Foundation of Jiangsu Provincial Department of Education (No. 17KJA430006). The support from Jiangsu overseas research & training program for university prominent young & middle-aged teachers is also acknowledged.

References

[1] K.S. Novoselov, D. Jiang, F. Schedin, T.J. Booth, V.V. Khotkevich, S.V. Morozov, A.K. Geim, Proc. Natl. Acad. Sci. Unit. States Am. 102 (2005) 10451–10453.
[2] B. Ouyang, P. Ou, Y. Wang, Z. Mi, J. Song, Phys. Chem. Chem. Phys. 18 (2016) 33351–33356.
[3] I. Sharma, B.R. Mehta, J. Alloy. Comp. 723 (2017) 50–57.
[4] X. Wang, K. Maeda, A. Thomas, K. Takanabe, G. Xin, J.M. Carlsson, K. Domen, M. Antonietti, Nat. Mater. 8 (2009) 76–80.
[5] J. Wen, J. Xie, X. Chen, X. Li, Appl. Surf. Sci. 391 (2017) 72–123.
[6] G. Liu, P. Niu, C. Sun, S.C. Smith, Z. Chen, G.Q. Lu, H.M. Cheng, J. Am. Chem. Soc. 132 (2010) 11642–11648.
[7] J.H. Sun, J.S. Zhang, M.W. Zhang, M. Antonietti, X.Z. Fu, X.C. Wang, Nat. Commun. (2012) 1139.
[8] R. Sun, Q. Shi, M. Zhang, L. Xie, J. Chen, X. Yang, M. Chen, W. Zhao, J. Alloys Compd. 714 (2017) 619–626.
[9] E. Kroke, M. Schwarz, Coord. Chem. Rev. 248 (2004) 493–532.
[10] A. Thomas, A. Fischer, F. Goettmann, M. Antonietti, J.-O. Muller, R. Schlogl, J.M. Carlsson, J. Mater. Chem. 18 (2008) 4893–4908.
[11] G.A. Siller, N. Severin, S.Y. Chong, T. Björkman, R.G. Palgrave, A. Laybourn, M. Antonietti, Y.Z. Khimyak, A.V. Krasheninnikov, J.P. Rabe, U. Kaiser, A.I. Cooper, A. Thomas, M.J. Bojdys, Angew. Chem. Int. Ed. 53 (2014) 7450–7455.
[12] J. Liu, J. Alloys Compd. 672 (2016) 271–276.
[13] J. Gracia, P. Kroll, J. Mater. Chem. 19 (2009) 3013–3019.
[14] E. Kroke, M. Schwarz, E. Horath-Bordon, P. Kroll, B. Noll, A.D. Norman, New J. Chem. 26 (2002) 508–512.
[15] X. Li, Y. Dai, Y. Ma, S. Han, B. Huang, Phys. Chem. Chem. Phys. 16 (2014) 4230–4235.
[16] H. Zhang, X. Zuo, H. Tang, G. Li, Z. Zhou, Phys. Chem. Chem. Phys. 17 (2015) 6280–6288.
[17] P. Niu, L. Zhang, G. Liu, H. Cheng, Adv. Funct. Mater. 22 (2012) 4763–4770.
[18] B. Kocak, Y.O. Ciftci, J. Alloy. Comp. 705 (2017) 211–217.
[19] S.P. Sun, X.P. Li, Y. Zhang, H.J. Wang, Y. Yu, Y. Jiang, D.Q. Yi, J. Alloy. Comp. 714 (2017) 459–466.
[20] X. Ma, Y. Lv, J. Xu, Y. Liu, R. Zhang, Y. Zhu, J. Phys. Chem. C 116 (2012) 23485–23493.
[21] S. Lu, C. Li, H.H. Li, Y.F. Zhao, Y.Y. Gong, L.Y. Niu, X.J. Liu, T. Wang, Appl. Surf. Sci. 392 (2017) 966–974.
[22] J. Cui, S. Liang, X. Wang, J. Zhang, Mater. Chem. Phys. 161 (2015) 194–200.
[23] G. Kresse, J. Furthmuller, Phys. Rev. B 54 (1996) 11169–11186.
[24] G. Kresse, J. Furthmuller, Comput. Mater. Sci. 6 (1996) 15–50.
[25] G. Kresse, D. Joubert, Phys. Rev. B 59 (1999) 1758–1775.
[26] J.P. Perdew, K. Burke, M. Ernzerhof, Phys. Rev. Lett. 77 (1996) 3865–3868.
[27] S. Grimme, J. Comput. Chem. 27 (2006) 1787–1799.
[28] J. Heyd, G.E. Scuseria, M. Ernzerhof, J. Chem. Phys. 124 (2006) 219906.
[29] H.J. Monkhorst, J.D. Pack, Phys. Rev. B 13 (1976) 5188–5192.
[30] S. Lin, X. Ye, X. Gao, J. Huan, J. Mol. Catal. Chem. 406 (2015) 137–144.
[31] D.M. Teter, R.J. Hemley, Science 271 (1996) 53–55.
[32] J. Luo, B. Wen, R. Melnik, Physica 45 (2012) 190–193.
[33] Q. Fan, C. Chai, Q. Wei, Y. Yang, Materials 9 (2016) 427.
[34] Y. Xu, S.P. Gao, Int. J. Hydrogen Energy 37 (2012) 11072–11080.
[35] B. Molina, L.E. Sansores, Mod. Phys. Lett. B 13 (1999) 193–201.
[36] L.W. Ruan, Y.J. Zhu, L.G. Qiu, Y.X. Lu, Vacuum 106 (2014) 79–85.
[37] M.J. Bojdys, J.O. Müller, M. Antonietti, A. Thomas, Chem. Eur J. 14 (2008) 8177–8182.
[38] H. Pan, J. Phys. Colloid Chem. 118 (2014) 9318–9323.
[39] J. Wirth, R. Neumann, M. Antonietti, P. Saalfrank, Phys. Chem. Chem. Phys. 16 (2014) 15917–15926.
[40] S.M. Aspera, M. David, H. Kasai, Jpn. J. Appl. Phys. 49 (2010) 115703–115712.
[41] L.W. Ruan, Y.J. Zhu, L.G. Qiu, Y.P. Yuan, Y.X. Lu, Comput. Mater. Sci. 91 (2014) 258–265.
[42] G.S. Manyali, R. Warmbier, A. Quandt, J.E. Lowther, Comput. Mater. Sci. 69 (2013) 299–303.
[43] Y.Z. Abdullahi, T.L. Yoon, M.M. Halim, M.R. Hashim, T.L. Lim, Solid State Commun. 248 (2016) 144–150.
[44] D. Ghosh, G. Periyasamy, S.K. Pati, J. Phys. Colloid Chem. 118 (2014) 15487–15494.
[45] Y. Liu, Y. Jiang, R. Zhou, J. Feng, Ceram. Int. 40 (2014) 2891–2899.
[46] R. Hill, Proc. Phys. Soc. A 65 (1952) 349–354.
[47] A. Liu, R. Wentzcovitch, Phys. Rev. B 50 (1994) 10362–10365.
[48] M.A. Blanco, E. Francisco, V. Luana, Comput. Phys. Commun. 158 (2004) 57–72.
[49] M. Forez, J.M. Recio, E. Francisco, M.A. Blanco, A.M. Pendas, Phys. Rev. B 66 (2002) 144112.
[50] E. Francisco, M.A. Blanco, G. Sanjurjo, Phys. Rev. B 63 (2001) 094107.
[51] S.P. Sun, X.P. Li, H.J. Wang, Y. Jiang, D.Q. Yi, J. Alloy. Comp. 652 (2015) 106–115.
[52] G.A. Slack, J. Phys. Chem. Sci. 34 (1973) 321–335.
[53] J. Feng, B. Xiao, R. Zhou, W. Pan, Acta Mater. 61 (2013) 7364–7383.
[54] B. Mortazavi, G. Cuniberti, T. Rabczuk, Comput. Mater. Sci. 99 (2015) 285–289.